Control Engineering Practice 114 (2021) 104877

Contents lists available at ScienceDirect

Control Engineering Practice

journal homepage: www.elsevier.com/locate/conengprac

Experimental evaluation of feedforward tuning rules

F. García-Mañas [a], J.L. Guzmán [a,*], F. Rodríguez [a], M. Berenguel [a], T. Hägglund [b]

[a] Department of Informatics, University of Almería, CIESOL, ceiA3, E04120 Almería, Spain
[b] Department of Automatic Control, Lund University, Box 118, SE-22100 Lund, Sweden

ARTICLE INFO

Keywords:
Feedforward
Disturbance rejection
Compensator design
Lead–lag filter
PID control
Greenhouse control

ABSTRACT

This paper presents a practical comparison for some of the most relevant tuning rules for feedforward compensators that have been published in the recent years. The work is focused on the rejection of disturbances that affect the process output. The different tuning rules are evaluated in simulation and several performance indices are calculated in order to provide a quantitative comparison. All the tuning rules are compared against a standard feedback controller and the classical open-loop design method for feedforward compensators. Furthermore, two of the analysed tuning rules are tested in a real process for the first time. To that end, a traditional greenhouse was selected as a test bed for an experimental evaluation of the feedforward controllers in the context of a challenging control problem with significant disturbances.

1. Introduction

Satisfactory disturbance rejection is one of the most prevalent existing problems in process control. Although feedback controllers can be tuned to attenuate the effects of disturbances, they present important limitations, so that suitable removal of the disturbance effect cannot be guaranteed. For this reason, the inclusion of a feedforward controller in a feedback control scheme helps to enhance the disturbance rejection action (Åström & Hägglund, 2006). In general, the aim of a feedforward controller is to compensate the effect of a measurable disturbance before it causes an undesired result on the process output. Nevertheless, feedforward control action can be also applied to improve setpoint tracking performance (Piccagli & Visioli, 2009; Rojas & Vilanova, 2009; Visioli, 2004), being a widely used technique for motion control (Boerlage et al., 2003; Lambrechts et al., 2005). However, the present work focuses on feedforward control to reject measurable disturbances that affect the process output.

The classical design method to obtain an ideal feedforward compensator consists of dividing the dynamical relationship of the disturbance and the process output by the dynamical relationship of the control signal and the process output, with reversed sign. However, it is not possible to apply this method in all cases because the compensator may be non-realizable due to causality or stability issues (Guzmán et al., 2012).

In recent years, new tuning rules for feedforward compensators have been published in the literature proposing innovative solutions to the problems and limitations of the classical design method for feedforward controllers (Guzmán & Hägglund, 2011; Hast & Hägglund, 2014; Rodríguez et al., 2020, 2013, 2014, 2016; Veronesi et al., 2017; Vilanova et al., 2009). In this sense, the majority of these new rules focus on the cases when ideal feedforward controllers are non-realizable, for example, due to problems in the delay inversion or to the presence of right-half plane zeros in the process dynamics. Additionally, these rules were also formulated to minimize error indices, such as the integral absolute error (IAE) or the integral square error (ISE). Moreover, some of the rules can reduce or remove the overshoot in the process output or even impose constraints in the high-frequency gain of a feedforward compensator.

Despite that all the previously cited tuning rules demonstrate important advances and improvements, the majority of them have been only evaluated in simulation studies, so there is a necessity of testing these design rules in real processes. For instance, the simple tuning rules in Guzmán and Hägglund (2011) were recently applied for the first time in a real process to control the air temperature inside a greenhouse, and favourable results were obtained (Montoya-Ríos et al., 2020).

In this context, the main contribution of the present work is the practical comparison of feedforward tuning rules applied to the problem of non-realizable delay inversion. To that end, some simulations are presented and numerous performance indices are provided for a quantitative comparison. For the experimental evaluation, two of the cited feedforward tuning rules were applied to a real control problem which is the regulation of the inside air temperature of a greenhouse.

The manuscript is organized as follows. Section 2 presents a summary of the feedforward tuning rules selected for this work. In Section 3, a series of performance indices are defined in order to compare the behaviour of the different feedforward compensators and control

* Corresponding author.
E-mail addresses: francisco.gm@ual.es (F. García-Mañas), joseluis.guzman@ual.es (J.L. Guzmán), frrodrig@ual.es (F. Rodríguez), beren@ual.es (M. Berenguel), tore.hagglund@control.lth.se (T. Hägglund).

https://doi.org/10.1016/j.conengprac.2021.104877
Received 25 January 2021; Received in revised form 2 June 2021; Accepted 16 June 2021
Available online xxxx

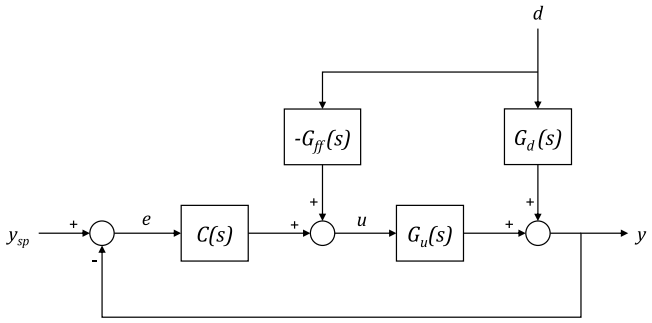

Fig. 1. Classical feedforward control scheme.

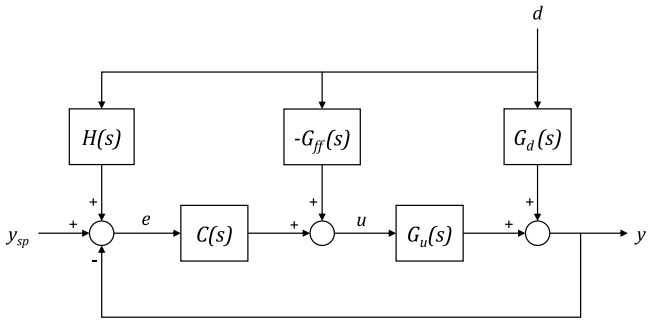

Fig. 2. Non-interacting feedforward control scheme.

schemes. In Section 4, the greenhouse temperature control is explained, the methodology to obtain the feedforward controllers for a real process is described, and simulated and real experimental results are discussed. Finally, Section 5 is dedicated to the conclusions of the work.

2. Summary of feedforward tuning rules

The classical feedforward control scheme in combination with a feedback controller $C(s)$ is shown in Fig. 1. According to this scheme, the ideal feedforward compensator can be calculated as follows:

$$G_{ff}(s) = \frac{G_d(s)}{G_u(s)} \tag{1}$$

where $G_u(s)$ is the transfer function relating the process output y to the control signal u and $G_d(s)$ is the transfer function that relates the measurable disturbance d to the process output. Thus, the feedforward compensator is calculated to remove the effect of the disturbance affecting the process output, so the feedforward action is added to the control signal coming from the feedback controller.

However, the ideal feedforward compensator presented in Eq. (1) could be non-realizable if the time delay in $G_u(s)$ is greater than the time delay in $G_d(s)$. With the classical design method, this realization problem is commonly solved by removing the delay term in $G_{ff}(s)$. Also, realization problems could appear due to the values of the poles and zeros in $G_u(s)$ and $G_d(s)$ (Rodríguez et al., 2014). Hence, the feedforward controller can be even reduced to a static gain (Åström & Hägglund, 2006). When the structure of the feedforward compensator needs to be approximated or modified as mentioned, a deteriorated control action is obtained since a perfect disturbance rejection is not achieved in the nominal case (Guzmán & Hägglund, 2011).

To improve the closed-loop control action when the ideal feedforward compensator is non-realizable, two different approaches can be found in the literature. The first approach consists of tuning the feedforward controller by taking into account the parameters of the feedback controller (Guzmán & Hägglund, 2011; Rodríguez et al., 2020; Veronesi et al., 2017). Notice that the classical method to calculate a feedforward compensator according to Eq. (1) is intended as an open-loop feedforward design, and the feedback controller is not considered for the design of the compensator. The second approach is based on a control scheme that allows the interaction of the feedback controller and the feedforward compensator to be decoupled (Hast & Hägglund, 2014; Rodríguez et al., 2013). This is achieved with the non-interacting control scheme presented in Brosilow and Joseph (2002), as shown in Fig. 2. The non-interacting scheme is obtained with the inclusion of the filter $H(s)$ determined with Eq. (2), which allows the measurable disturbance effect to be removed from the feedback error. Thereby, the feedback controller and the feedforward compensator can be tuned individually.

$$H(s) = G_d(s) - G_u(s)\, G_{ff}(s) \tag{2}$$

Apart from the two distinct approaches previously mentioned, some differences can be highlighted for each of the cited tuning rules. The simple tuning rules in Guzmán and Hägglund (2011) were formulated to obtain a disturbance rejection response with a minimum IAE value and without overshoot in the process output when applied to first-order systems. In Rodríguez et al. (2013), the tuning rules were generalized for the cases when delay inversion is not possible, proposing a series of methods to obtain an aggressive (minimizing ISE), a moderate (minimizing IAE), or a conservative (removing overshoot) response for the process output. The method formulated in Hast and Hägglund (2014) describes how to design low-order feedforward compensators to minimize the ISE for step disturbances. In Veronesi et al. (2017), two rules were proposed to tune the gain of a feedforward controller with the aim of reducing the overshoot in the response or minimizing the IAE. Finally, in Rodríguez et al. (2020), a series of tuning rules based on the internal model control (IMC) procedure were deduced to minimize the ISE, and these rules can be applied to a wide range of processes, with different types of disturbance signals.

All the aforementioned tuning rules have more considerations to improve the performance of the control action. For example, a switching feedforward tuning rule was proposed in Rodríguez et al. (2013) to provide fast responses with admissible control signal peaks, the concept of precompensation is used in Hast and Hägglund (2014), and a direct limitation of the high-frequency gain of the compensator is proposed in Guzmán and Hägglund (2011). Those considerations were out of the scope of the present work since it would require the analysis of different and more complex compensator structures.

Table 1 contains a summarized comparison for the tuning rules selected in this work. The column named as "Delay in compensator" is referred to the inclusion of the delay term in the feedforward compensator in case it is realizable. If the cell contains a "NO", it indicates that the rules are based on the assumption that the delay term is always removed due to inversion problems. Although some rules are designed for the non-interacting feedforward structure, it is possible to use them with a classical scheme, but some adjustments may be performed. For example, the compensator gain should be reduced as proposed in Guzmán and Hägglund (2011). In the present manuscript, the labels in Table 1 are utilized to identify in a simple manner each of the tuning rules when presenting or discussing the results of the work.

For an adequate comparison, in the present work, all the tuning rules are applied to a first-order plus deadtime (FOPDT) process, as presented in Eq. (3), with a PI controller tuned by the lambda method (Åström & Hägglund, 2006), which parameters are calculated with Eq. (6). The disturbance transfer function is also considered as an FOPDT process, according to Eq. (4). Hence, the feedforward compensators can be obtained as lead–lag filters, with the expression presented in Eq. (5).

$$G_u(s) = \frac{k_u}{\tau_u\, s + 1}\, e^{-L_u s} \tag{3}$$

$$G_d(s) = \frac{k_d}{\tau_d\, s + 1}\, e^{-L_d s} \tag{4}$$

Table 1
Comparison of the feedforward tuning rules selected for the present work.

Tuning rules	Label	Reference	Control structure	Delay in compensator	Min. IAE	Min. ISE	Reduce overshoot	No overshoot
Simple tuning rules	FF STr	Guzmán and Hägglund (2011)	Classical	YES	X			(AND) X
Generalized tuning rules	FF Gen	Rodríguez et al. (2013)	Non-interacting	YES	X	(OR) X		(OR) X
Low-order FF controllers	FF HH	Hast and Hägglund (2014)	Non-interacting	YES		X		
Closed-loop tuning rules	FF CL	Veronesi et al. (2017)	Classical	NO	X		(OR) X	(OR) X
IMC tuning rules	FF IMC	Rodríguez et al. (2020)	Classical	NO		X		

$$G_{ff}(s) = k_{ff}\,\frac{\tau_z\, s+1}{\tau_p\, s+1}\; e^{-L_{ff}\, s} \tag{5}$$

$$T_i = \tau_u \qquad k_p = \frac{\tau_u}{k_u(L_u+\lambda)} \tag{6}$$

Due to the fact that some of the rules in Table 1 were designed with the assumption that the time delay term is removed from the feedforward compensator, this work is focused on the comparison of the cited techniques when applied to the presence of delay inversion problems, i.e., $L_d < L_u$. In the following subsections, the mathematical expressions for each of the selected tuning rules are briefly presented. Only the design steps followed in the realization of this work are shown. The expressions are formulated according to the nomenclature presented in Figs. 1 and 2, as well as in Eqs. (3) to (6). For a more extensive explanation of each of the tuning rules, it is encouraged the reading of the references cited in Table 1.

2.1. Simple tuning rules

The following steps for the simple tuning rules (closed-loop option) are applied to obtain a feedforward compensator to minimize the IAE without presenting an overshoot in the response.

Step 1. Set $\tau_z = \tau_u$ and $L_{ff} = max(0, L_d - L_u)$.
Step 2. Calculate τ_p as:

$$\tau_p = \begin{cases} \tau_d & L_u - L_d \le 0 \\ \tau_d - \frac{L_u - L_d}{1.7} & 0 < L_u - L_d < 1.7\,\tau_d \\ 0 & L_u - L_d > 1.7\,\tau_d \end{cases}$$

Step 3. Calculate the compensator gain k_{ff} as:

$$k_{ff} = \frac{k_d}{k_u} - \frac{k_p}{T_i}\, IE$$

$$IE = \begin{cases} k_d\,(\tau_u - \tau_d + \tau_p - \tau_z) & L_d \ge L_u \\ k_d\,(L_u - L_d + \tau_u - \tau_d + \tau_p - \tau_z) & L_d < L_u \end{cases}$$

Step 4. End of design.

2.2. Generalized tuning rules

With the generalized open-loop tuning rules, three different types of feedforward controller can be obtained depending on the election in Step 3. For this work, the IAE minimization option was selected.

Step 1. Set $k_{ff} = k_d/k_u$, $\tau_z = \tau_u$ and $L_{ff} = max(0, L_d - L_u)$.
Step 2. Calculate $L_b = L_u - L_d$.
Step 3. Calculate α depending on the desired behaviour:

$$\alpha = \begin{cases} \frac{L_b}{2\,\tau_d\left(1-\sqrt{e^{-(L_b/\tau_d)}}\right)} & \text{aggressive (ISE minimization)} \\ 1.7 & \text{moderate (IAE minimization)} \\ 4 & \text{conservative (overshoot removal)} \end{cases}$$

Step 4. Set τ_p according to:

$$\tau_p = \begin{cases} \tau_d & L_b \le 0 \\ \tau_d - \frac{L_b}{\alpha} & 0 < L_b < 4\,\tau_d \\ 0 & L_b \ge 4\,\tau_d \end{cases}$$

If $\tau_p = 0$, select a value close to zero to obtain a realizable compensator.
Step 5. Set $H(s)$ with Eq. (2) for the non-interacting scheme.
Step 6. End of design.

2.3. Low-order feedforward controllers

The tuning rules to calculate low-order feedforward controllers are formulated to offer an optimal control by minimizing the ISE value. Additionally, some control signal considerations are also explained to avoid undesirable peaks.

Step 1. Calculate $L = L_u - L_d$.
Step 2. If $L < 0$, then set $L_{ff} = 0$.
Step 3. Set $k_{ff} = k_d/k_u$
Step 4. Calculate $a = \tau_u/\tau_d$ and $b = a(a+1)e^{L/\tau_d}$.
Step 5. Calculate τ_p as:

$$\tau_p = \begin{cases} \frac{3a-1-b+(a-1)\sqrt{1+4b}}{b-2}\,\tau_d & \text{If } b < 4a^2 - 2a \text{ or } b < a + \sqrt{a} \\ \tau_p = 0 & \text{Otherwise} \end{cases}$$

Step 6. Calculate τ_z as:

$$\tau_z = (\tau_p + \tau_u)\left(1 - \frac{2\tau_u}{b(\tau_d + \tau_p)}\right)$$

Step 7. If $\tau_p = 0$, the feedforward compensator is augmented with a second-order low-pass filter as follows:

$$G_{ff} = k_{ff}\,\frac{\tau_z\, s+1}{(\tau_f\, s+1)^2}\; e^{-L_{ff}\, s}$$

where τ_f is the time constant of the filter. To obtain a control signal with a peak of Δ value (being $\Delta > 1$), τ_f should be calculated with the following expression:

$$\tau_f = \frac{\tau_z}{1 + \frac{1}{W_0\left(\frac{e^{-1}}{\Delta-1}\right)}}$$

where W_0 is the principal branch of the LambertW function (Corless et al., 1996).
Step 8. Set $H(s)$ with Eq. (2) for the non-interacting scheme.
Step 9. End of design.

2.4. Closed-loop tuning rules

The closed-loop tuning rules are applied to the calculation of the feedforward compensator gain. The following steps correspond to the design rule for IAE minimization.

Step 1. Set $\tau_z = \tau_u$ and $\tau_p = \tau_d$.
Step 2. Calculate the compensator gain k_{ff} as:

$$k_{ff} = \frac{k_d\,(\tau_d + L_d)}{k_u\,(\tau_d + L_u)}$$

Step 3. End of design.

2.5. IMC tuning rules

The simplified internal model control tuning rules for feedforward controllers are deduced to minimize the ISE value by tuning only one parameter.

1. Set $\tau_z = \tau_u$ and $\tau_p = \tau_d$.
2. Calculate the compensator gain k_{ff} as:

$$k_{ff} = \frac{k_d}{k_u}\, e^{\frac{L_u - L_d}{\tau_\eta + \tau_d}}$$

where τ_η is the tuning parameter. This parameter can be equal to λ from Eq. (6) if a PI controller is selected as the feedback controller and its parameters are calculated with the lambda method.

3. End of design.

3. Performance indices

The performance of the feedforward tuning rules summarized in Table 1 can be superior with the classical or the non-interacting scheme, depending on the parameters of the process transfer function, the disturbance transfer function, and the value for the desired closed-loop time constant. This fact was mathematically demonstrated in Guzmán et al. (2015) for tuning rules such as the FF STr and the FF Gen. In the cited work, a performance index was proposed to evaluate the advantage of adding a feedforward compensator to a feedback controller. Theoretical estimations for the IAE were deduced considering a step disturbance. The ratio between the IAE value of the classical scheme and the non-interacting scheme was analysed. Based on the IAE estimation given in Guzmán and Hägglund (2011), it was concluded that the classical scheme gives a better performance when τ_d is large compared to process time delay L_u or to the desired closed-loop time constant λ.

Therefore, a series of performance indices are provided in this work for a quantitative comparison of the results presented in Section 4. The control action is analysed through the IAE, the ISE, the integral time absolute error (ITAE) and the integral time squared error (ITSE). Additionally, the maximum and minimum values for the control signal are presented. The control effort is quantified by means of an index calculated for the control signal according to the following expression:

$$J(u) = \sum_{k=t_{ON}+1}^{t_{OFF}} |u(k) - u(k-1)| \tag{7}$$

where $J(u)$ is the control effort index, u is the control signal, k represents the discrete-time instants, t_{ON} is the time instant when the automatic control was activated, and t_{OFF} is the time instant when the automatic control was disabled.

Also, the performance index proposed in Guzmán et al. (2015) has been utilized as a relative comparison of the feedforward control responses against the feedback controller response. This index is calculated as follows:

$$I_{FF/FB} = 1 - \frac{IAE_{FF}}{IAE_{FB}} \tag{8}$$

where IAE_{FF} is the integral absolute error obtained with a feedforward control strategy and IAE_{FB} is the integral absolute error obtained with the feedback controller without the inclusion of a feedforward compensator. If the feedforward action removes the effect of the disturbance, IAE_{FF} is equal to 0 and the index $I_{FF/FB}$ is equal to 1. If the feedforward action improves the control response, the index is close to 1, because $IAE_{FF} < IAE_{FB}$.

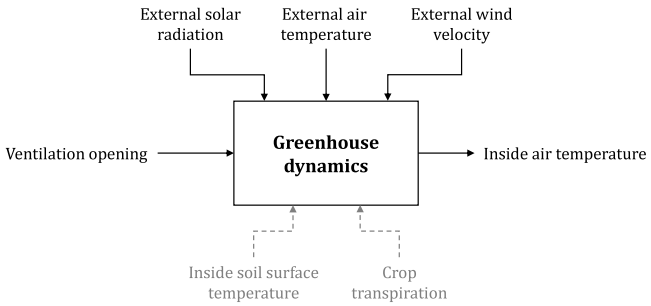

Fig. 3. Schematic representation of the variables affecting the inside air temperature of a greenhouse.

4. Experimental study

Once the different feedforward solutions have been summarized, an extensive experimental study is presented for the feedforward tuning rules cited in Table 1. In the coming subsections, the greenhouse temperature control problem is explained, the real facilities are briefly described and real sensor data are utilized to calculate low-order models of the process in order to design the different feedforward compensators. Moreover, specific simulation studies are executed for a better understanding of the benefits of applying a feedforward control to the real greenhouse. Then, the results of testing the FF CL and the FF IMC tuning rules at the real greenhouse are analysed.

4.1. Greenhouse temperature control problem

Climate control for greenhouses is a key aspect to achieve an optimal crop production (Rodríguez et al., 2015). During the daytime hours, and depending on the geographical location of the greenhouse, the regulation of the inside air temperature in adequate ranges for the crop can be a difficult task. In Fig. 3, some of the variables affecting the inside air temperature of a greenhouse are shown. From the perspective of a disturbance rejection problem, a greenhouse offers a challenging scenario, since the external weather conditions can be considered as measurable disturbances that affect the evolution of the inside climate variables. Also, the inside soil surface temperature could be treated as a measurable disturbance acting like a thermal inertia for the process, but it was not contemplated for this work since its evolution in time is considerably slower compared to the external weather disturbances and its influence is higher during the nocturnal periods. Additionally, although the crop transpiration affects the inside climate, this variable is assumed as a non-measurable disturbance that is compensated by the feedback controller.

The control problem proposed for the experimental evaluation of the feedforward tuning rules consists of controlling the inside air temperature of a greenhouse during the daytime by regulating the opening of the natural ventilation system. Considering that the inside air temperature of a greenhouse is normally higher than the external air temperature, when the vents of the greenhouse are opened, the warmer air inside the greenhouse is evacuated through the roof vents because it is less dense than the outdoor cooler air entering through the lateral vents of the cover.

This control problem has been faced in the past with different control approaches (Berenguel et al., 2003; Gruber et al., 2011; Iddio et al., 2020; del Sagrado et al., 2016), even including feedforward control (Fourati & Chtourou, 2007; Gurban & Andreescu, 2012; Pawlowski et al., 2012; Rodríguez et al., 2001). Recently, the simple tuning rules in Guzmán and Hägglund (2011) were successfully applied to this problem in a real greenhouse (Montoya-Ríos et al., 2020). In view of the promising results that were obtained, the same greenhouse has been selected as a test bed for the current work.

(a) (b) (c)

Fig. 4. Experimental greenhouse. (a) Exterior view in which a roof and a lateral window are observed. (b) Interior crop area. (c) Inside air temperature sensor.

Table 2
Transfer functions calculated in November 2020 for the greenhouse dynamics. Time constants and time delays are expressed in seconds. Disturbance d_1 is the external solar radiation, disturbance d_2 is the external air temperature, and disturbance d_3 is the external wind velocity.

	Units	15 November 2020	16 November 2020	Average
$G_u(s)$	$\left[\frac{°C}{\%}\right]$	$\frac{-0.09656}{2731\ s+1}\ e^{-221\ s}$	$\frac{-0.06535}{1710\ s+1}\ e^{-376\ s}$	$\frac{-0.08095}{2220\ s+1}\ e^{-298\ s}$
$G_{d1}(s)$	$\left[\frac{°C}{W/m^2}\right]$	$\frac{0.01709}{2724\ s+1}\ e^{-225\ s}$	$\frac{0.01159}{1682\ s+1}\ e^{-263\ s}$	$\frac{0.01434}{2203\ s+1}\ e^{-244\ s}$
$G_{d2}(s)$	$\left[\frac{°C}{°C}\right]$	$\frac{1.141}{2725\ s+1}\ e^{-268\ s}$	$\frac{1.191}{1746\ s+1}\ e^{-207\ s}$	$\frac{1.166}{2236\ s+1}\ e^{-238\ s}$
$G_{d3}(s)$	$\left[\frac{°C}{m/s}\right]$	$\frac{-0.2068}{2327\ s+1}$	$\frac{-0.3658}{1879\ s+1}\ e^{-285\ s}$	$\frac{-0.2863}{2103\ s+1}\ e^{-143\ s}$

4.2. Greenhouse description

Control tests for this work were performed in a traditional Mediterranean greenhouse located in Almería, in the southeast of Spain. This greenhouse (see Fig. 4) is a facility situated at the Experimental Station "Las Palmerillas", property of the Cajamar Foundation. The total surface of the greenhouse is 877 m^2 and it is equipped with different actuators to regulate the climate under the cover. For the present work, only the natural ventilation system was utilized. This system is based on two lateral windows (32.75 m × 1.90 m) and five roof windows (8.36 m × 0.73 m), which can be opened by using three AC motors (2 × 0.18 kW and 1 × 0.37 kW). These motors receive an electrical current lasting a specific time period to open or close the windows in a desired percentage (from 0% to 100%).

Advanced monitoring devices are installed inside and outside the greenhouse to register the internal and external climate conditions. Real experimental data for this work were provided by the following sensors. The inside and outside air temperature are measured with protected temperature probes, model HC2S3 (Campbell Scientific Ltd., Shepshed, UK). A pyranometer, model LP02 (Hukseflux, Delft, The Netherlands), is used to register the external global solar radiation. An anemometer, model A100L2 (Vector Instruments, Rhyl, UK), measures the external wind velocity. All the sensors data are recorded with a sampling period of 30 s.

4.3. Low-order models for control purposes

The climate under the cover of a greenhouse is a result of multiple energy transfers and mass balances, and the dynamical evolution of the variables affecting the crop is usually expressed by complex non-linear models (Rodríguez et al., 2015). Using these models to analytically calculate a controller might be an arduous task. Therefore, system identification techniques are usually employed as an easier alternative to calculate simplified models based on measured data from the real process. Specifically, in this work, the methodology described in Montoya-Ríos et al. (2020) has been followed to obtain transfer function models to represent the dynamics of the greenhouse. This methodology is summarized in the next points and it can be comfortably performed, for example, with the System Identification Toolbox™ in MATLAB® (The MathWorks, MA, USA):

1. Identification of high-order auto-regressive with exogenous input (ARX) models.
2. Simulation of unit steps as inputs for the ARX models to obtain the step responses of the process output.
3. Identification of low-order transfer functions for each of the simulated step responses.
4. Calculation of the feedback controller and the feedforward compensators based on the transfer function models.

The identification of ARX models was accomplished by selecting a series of datasets with real data from different days of November 2020. In all days, the signal for the ventilation opening was generated intentionally to excite the system during the daytime. The excitation of the manipulated input created noticeable changes in the process output (inside air temperature). Various ARX models were identified during the first two weeks of November and the best results were achieved with data from days 15 and 16 of November 2020. The goodness of fitting to the real data was graphically confirmed, as shown in Fig. 5. For reasons of limited space, graphical results for day 16 November 2020 are not presented. For day 15 November 2020, the mean absolute error (MAE) is 0.45 °C, the maximum absolute error (MaxAE) is 1.28 °C and the standard deviation (SD) is 0.37 °C. For day 16 November 2020, the MAE is 0.38 °C, the MaxAE is 1.28 °C and the SD is 0.39 °C.

Considering that a greenhouse is a system with strong disturbances, its dynamical behaviour can drastically change from a sunny day to a cloudy day, for example. For this reason, individual ARX models were obtained for each day instead of calculating only one ARX model for some continuous days. By this manner, the intention was to have different ARX models that could capture with more accuracy the dynamical behaviour of the process, especially during the daytime.

For the two ARX models, unit steps were given as inputs and low-order models were identified as transfer functions (presented in Table 2), with an excellent adjustment to the simulated step responses for both days. However, the values for the parameters are different for each day, mainly for the time constants and the time delays. To take into account the variability that exists in the days prior to the control tests, the average transfer functions for both days were selected as the low-order models for the design of the feedback controller and the feedforward compensators. Thus, it is assumed that the average transfer functions are a reliable representation of the real dynamics. Nevertheless, the validity of these linear models for a non-linear system such as a greenhouse depends on the operational conditions. Hence, as a disadvantage of the followed procedure, it is imperative to recalculate the models for different states of the crop and for different seasons of the year, depending on how often the external weather conditions vary at the location of the greenhouse. As an alternative, several techniques could be applied to achieve the regular identification of the low-order

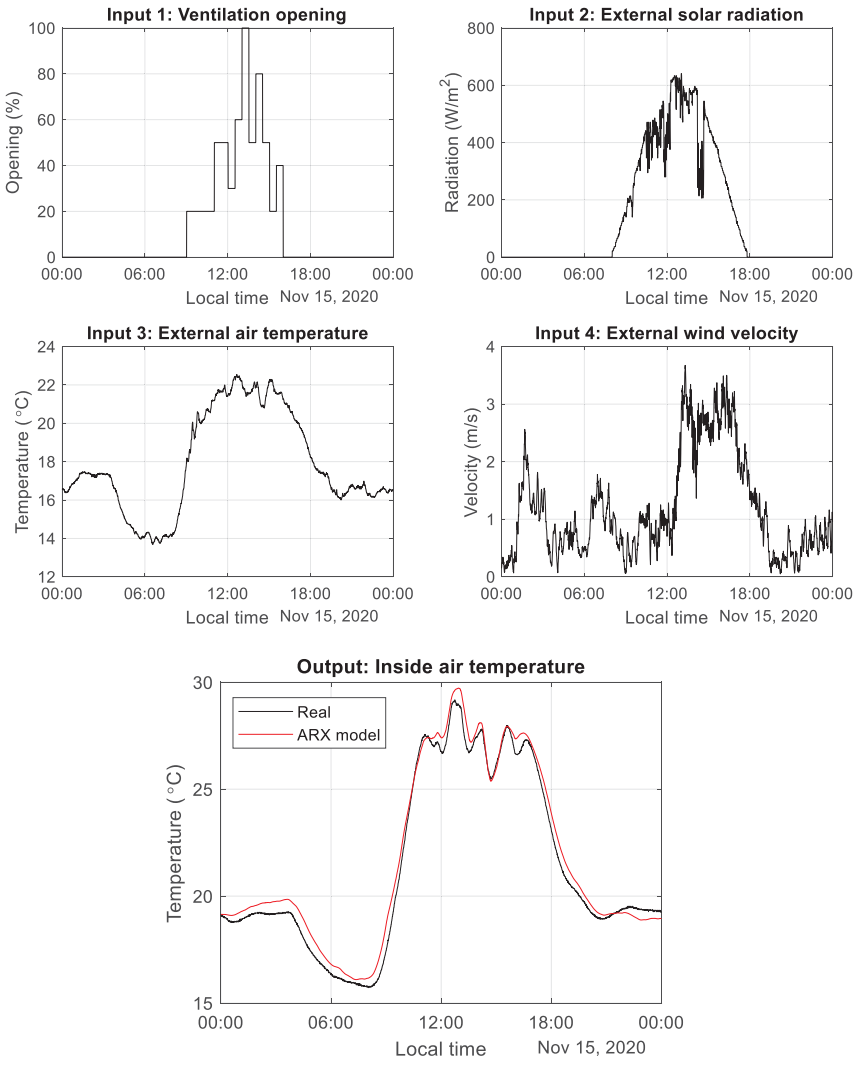

Fig. 5. Results for ARX model identification with data from 15 November 2020.

models and even the adjustment of the controllers by using closed-loop operating data, without the need of performing specific identification tests (Berenguel et al., 2003; Speetjens et al., 2009; Su et al., 2020; Veronesi & Visioli, 2014).

4.4. Calculation of the feedback controller and the feedforward compensators

The complete control scheme proposed in this work to control the air temperature inside the greenhouse is shown in Fig. 6. The three main external disturbances have been taken into account as explained in Section 4.1 and the respective feedforward compensators are included with the classical disposition (see Fig. 1). The $H_i(s)$ filters are also considered for the non-interacting scheme (see Fig. 2), represented in dashed grey lines, and they were only utilized with the corresponding tuning rules according to Table 1.

The feedback controller was calculated as a PI controller by applying the lambda tuning method to the average process transfer function $G_u(s)$ from Table 2. The tuning parameter was fixed as $\lambda = 0.3\,\tau_u$, resulting in a value of 666.09 s. With this value for λ, the feedback controller is expected to compensate the effect of non-measurable disturbances and other uncertainties caused by modelling errors. Using Eq. (6), the resulting parameters for the PI controller are $k_p = -28.44\%/°C$ and $T_i = 2220$ s. Moreover, the feedback controller is also combined with an anti-windup mechanism, with a tracking constant calculated as $T_t = \sqrt{T_i}$. This solution is needed to deal with the physical limits of the natural ventilation system, since the opening range of the vents is logically restricted from 0% to 100%. It is also important to remark that a minimum amplitude of 10% is required for the control signal every time the ventilation motors are activated. This limitation of the real process is also taken into consideration for the simulation tests in Section 4.6.

The calculation of the feedforward compensators has been achieved by using the average transfer functions from Table 2 and the mentioned PI parameters. The resulting feedforward compensators are shown in Table 3. All the feedforward controllers were calculated without the presence of the time delay term, since the transfer functions describing the greenhouse dynamics presented the problem of non-realizable delay inversion. Therefore, the resulting lead–lag filters are very similar, but with some minor differences in the values of the poles and zeros. A special case occurs with the FF HH tuning rules. The second low-pass filter from Step 7 in Section 2.3 was necessarily added to calculate the compensators for the external solar radiation and the external air temperature. The time constant of the filter was calculated by limiting the control signal peak to $\Delta = 1.3$. The election of this value is discussed in the next sections.

4.5. Simulation tests with transfer functions

Before testing the feedforward controllers with real data or at the real greenhouse, some simulations were executed to understand how

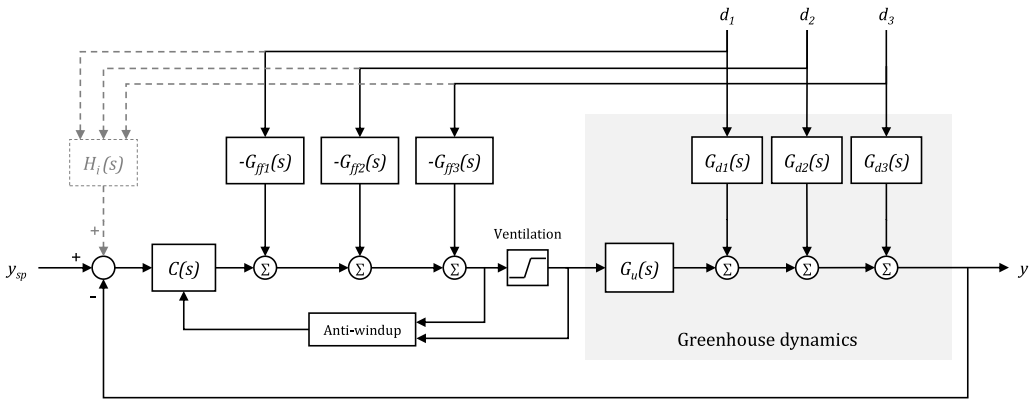

Fig. 6. Greenhouse inside air temperature control scheme.

Table 3
Feedforward compensators calculated in November 2020 for the greenhouse dynamics.

	Ext. radiation (G_{ff1})	Ext. temperature (G_{ff2})	Ext. wind velocity (G_{ff3})
FF classical	$\frac{-393.2\ s - 0.1771}{2203\ s + 1}$	$\frac{-3.197 \cdot 10^4\ s - 14.4}{2236\ s + 1}$	$\frac{7852\ s + 3.537}{2103\ s + 1}$
FF STr	$\frac{-384.1\ s - 0.1730}{2171\ s + 1}$	$\frac{-3.115 \cdot 10^4\ s - 14.03}{2200\ s + 1}$	$\frac{7331\ s + 3.302}{2012\ s + 1}$
FF Gen	$\frac{-393.2\ s - 0.1771}{2171\ s + 1}$	$\frac{-3.197 \cdot 10^4\ s - 14.4}{2200\ s + 1}$	$\frac{7852\ s + 3.537}{2012\ s + 1}$
FF HH	$\frac{-11.04\ s - 0.1771}{24.42\ s^2 + 48.83\ s + 1}$	$\frac{-744.4 \cdot 10^4\ s - 14.4}{20.25\ s^2 + 40.5\ s + 1}$	$\frac{983.3\ s + 3.537}{60.85\ s + 1}$
FF CL	$\frac{-384.7\ s - 0.1733}{2203\ s + 1}$	$\frac{-3.121 \cdot 10^4\ s - 14.06}{2236\ s + 1}$	$\frac{7344\ s + 3.307}{2103\ s + 1}$
FF IMC	$\frac{-385.8\ s - 0.1738}{2203\ s + 1}$	$\frac{-3.131 \cdot 10^4\ s - 14.1}{2236\ s + 1}$	$\frac{7423\ s + 3.343}{2103\ s + 1}$

Table 4
Performance indices for the control responses to reject step disturbances affecting the greenhouse dynamics.

External radiation disturbance								
	IAE	ISE	ITAE	ITSE	max(u)	min(u)	J(u)	$I_{FF/FB}$
PI	962.33	164.909	$3.94 \cdot 10^6$	$5.27 \cdot 10^5$	12.36	0	**12.37**	–
FF classical	29.05	**0.293**	$9.90 \cdot 10^4$	559.10	13.13	0	13.94	0.9698
FF STr	22.38	0.304	$6.88 \cdot 10^4$	**500.70**	13.01	0	13.73	0.9767
FF Gen	33.68	0.386	$1.12 \cdot 10^5$	741.32	12.63	0	12.93	0.9650
FF HH	57.64	0.569	$2.34 \cdot 10^5$	1583.72	15.71	0	19.42	0.9401
FF CL	22.44	0.364	$\mathbf{4.54 \cdot 10^4}$	604.77	12.93	0	13.52	0.9767
FF IMC	**22.33**	0.345	$4.95 \cdot 10^4$	568.98	12.95	0	13.57	**0.9768**
External temperature disturbance								
	IAE	ISE	ITAE	ITSE	max(u)	min(u)	J(u)	$I_{FF/FB}$
PI	962.46	163.130	$3.96 \cdot 10^6$	$5.23 \cdot 10^5$	12.35	0	**12.35**	–
FF classical	32.05	**0.355**	$1.10 \cdot 10^5$	675.80	13.06	0	13.78	0.9667
FF STr	24.84	0.369	$7.69 \cdot 10^4$	**608.32**	12.92	0	13.59	0.9742
FF Gen	37.53	0.473	$1.26 \cdot 10^5$	910.54	12.47	0	12.59	0.9610
FF HH	35.01	0.402	$9.79 \cdot 10^4$	819.81	15.71	0	19.32	0.9636
FF CL	24.67	0.439	$\mathbf{4.98 \cdot 10^4}$	727.54	12.84	0	13.35	0.9744
FF IMC	**24.56**	0.416	$5.44 \cdot 10^4$	685.11	12.87	0	13.41	**0.9745**
External wind velocity disturbance								
	IAE	ISE	ITAE	ITSE	max(u)	min(u)	J(u)	$I_{FF/FB}$
PI	962.18	170.74	$3.75 \cdot 10^6$	$5.19 \cdot 10^5$	0	−12.50	**12.65**	–
FF classical	86.13	2.523	$2.84 \cdot 10^5$	$4.73 \cdot 10^3$	0	−15.04	17.82	0.9105
FF STr	**64.84**	2.539	$1.91 \cdot 10^5$	$4.06 \cdot 10^3$	0	−14.65	17.12	**0.9326**
FF Gen	96.92	3.289	$3.08 \cdot 10^5$	$6.08 \cdot 10^3$	0	−13.62	14.91	0.8993
FF HH	77.95	**0.928**	$4.24 \cdot 10^5$	$\mathbf{3.10 \cdot 10^3}$	0	−56.39	100.55	0.9190
FF CL	66.02	3.075	$\mathbf{1.28 \cdot 10^5}$	$4.99 \cdot 10^3$	0	−14.29	16.33	0.9314
FF IMC	65.50	2.894	$1.41 \cdot 10^5$	$4.64 \cdot 10^3$	0	−14.40	16.54	0.9319

the proposed control strategies (see Fig. 6) perform with the dynamics of the greenhouse, considering step and ramp disturbances affecting the process output. The step-like disturbances usually appear in the real process for the external solar radiation and the external wind velocity, when rapid and sudden changes occurs, such as clouds passing over the greenhouse. The ramp-like disturbances are more common for the external air temperature, with a more progressive evolution.

The dynamics of the greenhouse were simulated with the average transfer functions from Table 2. Since linearized models are being used, all the graphical results represent a change in the deviation variables. In this sense, the amplitude of the disturbances was calculated to create a unit deviation of the process output in open-loop. In order to focus on the comparison for the feedforward tuning rules, the PI controller responses are omitted in all the graphs since its disturbance rejection action is not satisfactory.

Fig. 7 shows the control responses to reject step disturbances affecting the greenhouse dynamics and the corresponding performance indices are presented in Table 4. The graphical and numerical results confirm that the tuning rules based on closed-loop techniques (FF STr, FF CL and FF IMC) offer the best performance to reject the three step disturbances, outperforming the classical feedforward method. The tuning rules based on the non-interacting scheme (FF Gen and FF HH) present a slower rejection action, with greater ITAE values.

Attending to the control signals, the differences between all the tuning rules are minimal. However, the small appreciable variations for the control signal in the first time instants crucially condition the evolution of the process output response to reject the step disturbances. Regarding the control effort index $J(u)$, the FF HH rules present the greatest control effort in all the cases, due to the appearance of peaks in the control signal. The limitation of those peaks was accomplished by adjusting $\Delta = 1.3$ to obtain a control signal with similar magnitude to the other tuning rules for an adequate comparison, but it was only possible for the external radiation and external air temperature disturbances. The behaviour of the FF HH was expected to be different for the external wind velocity disturbance, since the corresponding compensator has contrasting values for the pole and zero, compared to the other compensators (see Table 3). In this sense, the FF HH tuning rules are the only rules that consider the adjustment of τ_z (see Step 6 in Section 2.3), instead of assuming $\tau_z = \tau_u$. In some cases, the possibility of tuning the value for τ_z could be an advantage, but it could also provoke aggressive control signals (Hast & Hägglund, 2014).

The majority of the feedforward tuning rules were originally formulated to deal with step disturbances. However, in this simulation study, the feedforward compensators were also tested to reject ramp disturbances. Notice that the structures of the feedback controller and feedforward compensators are not modified. In this sense, it is recommended to increase the order of the feedback controller when the disturbance follows a ramp function (Rodríguez et al., 2020).

Fig. 8 shows the control responses to reject ramp disturbances affecting the greenhouse dynamics and Table 5 contains the corresponding performance indices. Surprisingly, the FF classical tuning rule

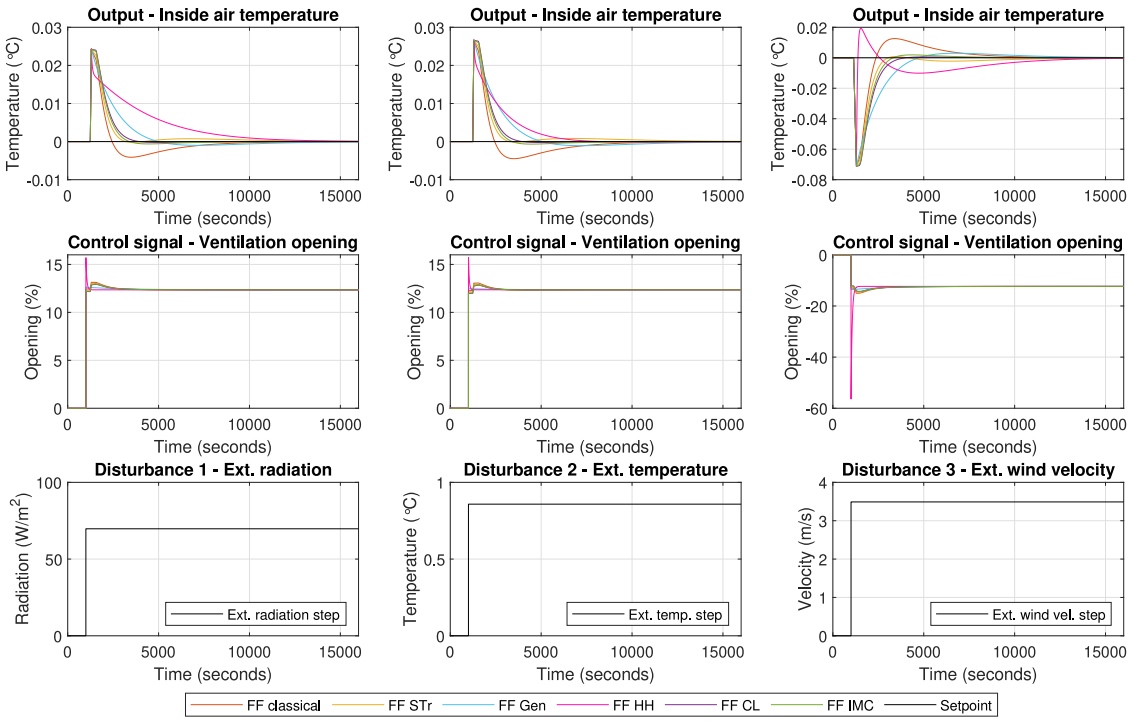

Fig. 7. Control responses to reject step disturbances affecting the greenhouse dynamics. The results represent a change in the deviation variables.

is the only technique rejecting the measurable disturbance and thus obtaining the best performance indices. This result means that the FF classical tuning rule, based on the classical control scheme, allows to completely reject ramp-like disturbances without the need of modifying the structure of the feedback controller. This can be demonstrated by analysing the resulting transfer function from the disturbance to the error, calculated for the classical control scheme in Fig. 1:

$$T(s) = -\frac{G_d(s) - G_u(s)\,G_{ff}(s)}{1 + G_u(s)\,C(s)} \tag{9}$$

where the compensator $G_{ff}(s)$ is designed with the classical rule assuming $L_{ff} = 0$, $\tau_z = \tau_u$, $\tau_p = \tau_d$, and the controller $C(s)$ is calculated with the lambda method. Hence, the transfer function is reduced to:

$$T(s) = -\frac{T_i\, s\,(k_d\, e^{-L_d\, s} - k_u\, k_{ff}\, e^{-L_u\, s})}{(T_i\, s + k_u\, k_p\, e^{-L_u\, s})\,(\tau_d\, s + 1)} \tag{10}$$

When the classical feedforward tuning rule is used, the compensator gain is not modified and it is calculated as $k_{ff} = k_d/k_u$, obtaining:

$$T(s) = -\frac{k_d\, T_i\, s\,(e^{-L_d\, s} - e^{-L_u\, s})}{(T_i\, s + k_u\, k_p\, e^{-L_u\, s})\,(\tau_d\, s + 1)} \tag{11}$$

Considering a ramp disturbance with k_r slope and applying the final value theorem, the steady-state error can be calculated as follows:

$$e(\infty) = \lim_{s\to 0}\, s \cdot E(s) = \lim_{s\to 0}\, s \cdot T(s) \cdot \frac{k_r}{s^2} = 0 \tag{12}$$

Notice that for the rest of the closed-loop tuning rules based on the classical control scheme, non-zero steady-state error is obtained because the feedforward gain is modified and, in consequence, ramp signals are not totally rejected. For instance, this is observed in Fig. 8 for the FF CL and the FF IMC tuning rules.

After analysing all the simulation results, it can be concluded that the FF STr, the FF CL and the FF IMC give, in the majority of the cases, lower IAE values with less control effort. Nonetheless, this performance had to be validated in simulations with real data before deciding the tuning rules that should be tested at the real greenhouse. A negative aspect for the FF STr can be remarked considering that the ITAE values with these tuning rules are greater than the ITAE values for the FF CL and the FF IMC. Graphically, this behaviour is corroborated for the FF STr since its transient responses take longer to reach the null error in steady state for step disturbances.

In general, the non-interacting scheme presents greater errors (see results with the FF Gen). As discussed in Section 3, this can be justified by the fact that the classical scheme gives a better performance when

Table 5
Performance indices for the control responses to reject ramp disturbances affecting the greenhouse dynamics.

External radiation disturbance								
	IAE	ISE	ITAE	ITSE	max(u)	min(u)	J(u)	$I_{FF/FB}$
PI	764.20	44.32	$7.52{\cdot}10^6$	$4.59{\cdot}10^5$	11.62	0	**11.62**	–
FF classical	**3.47**	**0.002**	$\mathbf{1.43{\cdot}10^4}$	**6.92**	12.41	0	12.41	**0.9955**
FF STr	19.08	0.025	$1.76{\cdot}10^5$	244.4	12.39	0	12.39	0.9750
FF Gen	23.23	0.038	$2.03{\cdot}10^5$	327.92	12.39	0	12.39	0.9696
FF HH	45.86	0.156	$4.47{\cdot}10^5$	1617.77	12.36	0	12.36	0.9400
FF CL	19.93	0.028	$1.77{\cdot}10^5$	246.41	12.39	0	12.39	0.9739
FF IMC	17.69	0.022	$1.55{\cdot}10^5$	188.50	12.39	0	12.39	0.9769
External temperature disturbance								
	IAE	ISE	ITAE	ITSE	max(u)	min(u)	J(u)	$I_{FF/FB}$
PI	762.76	44.17	$7.51{\cdot}10^6$	$4.58{\cdot}10^5$	11.60	0	**11.60**	–
FF classical	**3.87**	**0.003**	$\mathbf{1.60{\cdot}10^4}$	**8.54**	12.39	0	12.39	**0.9949**
FF STr	21.22	0.031	$1.95{\cdot}10^5$	302.88	12.37	0	12.37	0.9722
FF Gen	25.92	0.047	$2.27{\cdot}10^5$	408.86	12.37	0	12.37	0.9660
FF HH	30.52	0.066	$2.82{\cdot}10^5$	633.72	12.36	0	12.36	0.9600
FF CL	21.94	0.033	$1.94{\cdot}10^5$	298.42	12.37	0	12.37	0.9712
FF IMC	19.48	0.026	$1.70{\cdot}10^5$	228.68	12.37	0	12.37	0.9745
External wind velocity disturbance								
	IAE	ISE	ITAE	ITSE	max(u)	min(u)	J(u)	$I_{FF/FB}$
PI	776.56	45.28	$7.58{\cdot}10^6$	$4.64{\cdot}10^5$	0	−11.77	**11.77**	–
FF classical	**9.98**	**0.018**	$\mathbf{3.96{\cdot}10^4}$	**57.18**	0	−12.57	12.57	**0.9872**
FF STr	55.44	0.214	$5.08{\cdot}10^5$	2043.21	0	−12.51	12.51	0.9286
FF Gen	66.73	0.311	$5.80{\cdot}10^5$	2665.55	0	−12.51	12.51	0.9141
FF HH	33.38	0.101	$3.66{\cdot}10^5$	1184.95	0	−12.52	12.52	0.9570
FF CL	59.62	0.246	$5.28{\cdot}10^5$	2198.36	0	−12.52	12.52	0.9232
FF IMC	51.84	0.185	$4.51{\cdot}10^5$	1606.91	0	−12.52	12.52	0.9332

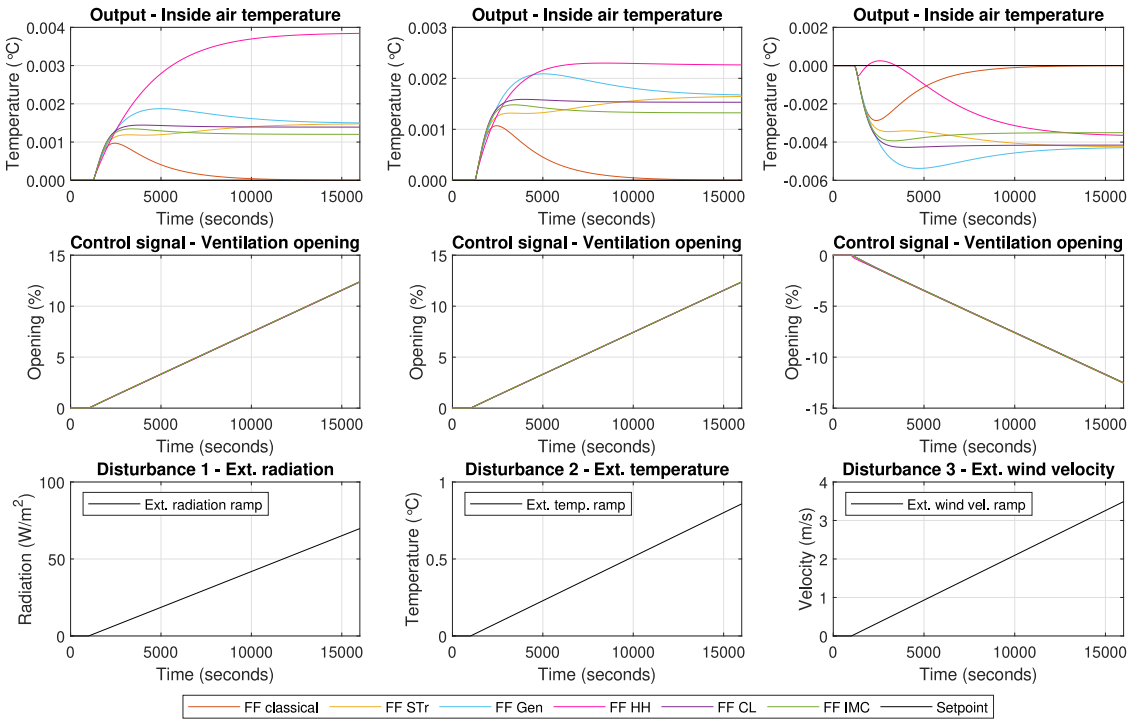

Fig. 8. Control responses to reject ramp disturbances affecting the greenhouse dynamics. The results represent a change in the deviation variables.

τ_d is large compared to the process delay time L_u or to the closed-loop time constant λ, which is the case of the greenhouse dynamics according to the transfer function models in Table 2.

4.6. Simulation tests with real data

The last stage before testing the feedforward tuning rules in the real process was to simulate the behaviour of the compensators with real data measured at the greenhouse. These simulations were performed to have a more accurate idea of how the proposed control strategies can perform when the disturbances are a real evolution of the external weather variables instead of isolated steps and ramps.

The control scheme proposed in Fig. 6 was implemented in Simulink® to execute the simulations. In this case, the greenhouse dynamics was simulated by the ARX models calculated in Section 4.3. The Simulink® model included a code function to imitate the real limitation of a minimum change of 10% in the control signal to activate the ventilation motors. The sample time for the Simulink® model was established as 30 s (fixed-step), matching the real sample time of the measured data.

The objective with these simulations was also to recreate the procedure to control the inside air temperature of the real greenhouse during the daytime. Considering that in the real process different controllers can be programmed for night and day, a bumpless transfer mechanism should be included (Åström & Hägglund, 2006; Montoya-Ríos et al., 2020). This mechanism was activated for the PI controller in the Simulink® model, allowing a smooth switching between controllers. The activation and deactivation of the daytime controller is shown in all the results graphs with the "Control ON" and "Control OFF" indicators.

Before presenting the results, it is important to remark that the same simulations with real data were executed for the FF HH and these rules were discarded to be tested in the real process due to the risk of presenting a very changing control signal that could damage the actuators.

The first simulation test was performed with data from 15 November 2020, as shown in Fig. 9. The results present an improved performance for the feedforward techniques compared to the PI controller without the feedforward compensators. The error gap graph shows that the feedforward control maintains the inside air temperature almost on the desired setpoint despite the important disturbances, especially at 13:00 for the external wind velocity and at 12:20 or at 14:10 for the external solar radiation. In those cases, the PI controller cannot reject the disturbances and the process output deviates from the setpoint. The feedforward actions can be observed in the control signal graph and they are particularly adequate at 14:10, when the ventilation is rapidly closed to prevent a drop in the inside air temperature.

Table 6
Performance indices for simulation with data from 15 November 2020.

	IAE	ISE	ITAE	ITSE	max(u)	max(Δu)	J(u)	E [kWh]
PI	12 616	12 097	$1.673 \cdot 10^8$	$1.663 \cdot 10^8$	80	10	**260**	**0.060**
FF classical	7731.6	7259.1	$8.908 \cdot 10^7$	$8.756 \cdot 10^7$	90	20	1540	0.354
FF STr	7604.7	7228.8	$8.814 \cdot 10^7$	$8.776 \cdot 10^7$	90	20	1540	0.354
FF Gen	7580.2	7261.7	$8.817 \cdot 10^7$	$8.851 \cdot 10^7$	90	20	1540	0.354
FF CL	**7522.1**	**7185.5**	$\mathbf{8.717 \cdot 10^7}$	$8.740 \cdot 10^7$	90	30	1500	0.345
FF IMC	7564.3	7196.1	$8.749 \cdot 10^7$	$\mathbf{8.737 \cdot 10^7}$	90	30	1460	0.336

The graphical results are very similar for all the tuning rules. For an easier comparison, the performance indices for these results are shown in Table 6. In this test, the FF CL and the FF IMC offer the lowest error values with a reduced control effort. The response of the PI controller presents the lowest control effort because its control signal is significantly less variant and, consequently, the IAE value reveals its bad performance. Additionally, an estimated energy consumption index, E, has been included to compare the accumulated electricity consumption (in kWh) during the control interval for each of the simulated control strategies. This index is calculated based on the power consumption of the ventilation motors (see Section 4.2). Attending to this energy index, the tuning rules consuming less electricity (FF CL and FF IMC) will offer lower operational costs for a real greenhouse.

The second simulation was accomplished with real data from 16 November 2020, as presented in Fig. 10. In this case, the external weather disturbances present less variations affecting the inside air temperature. Nonetheless, the feedforward control overcomes again the

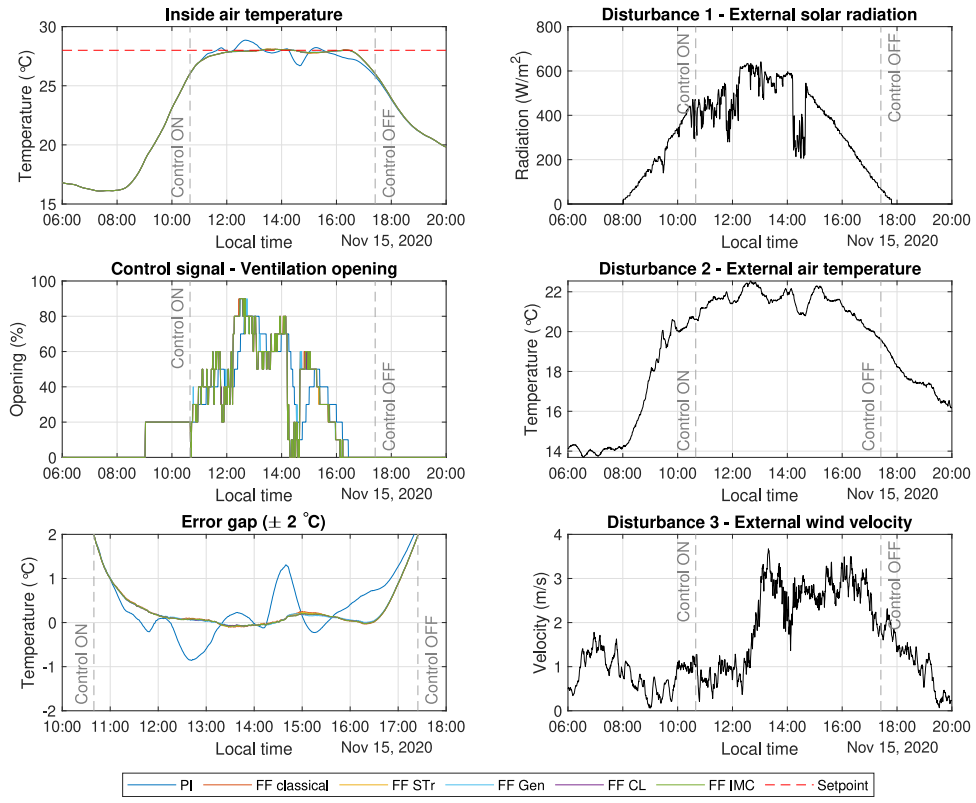

Fig. 9. Results for simulation with data from 15 November 2020.

Table 7
Performance indices for simulation with data from 16 November 2020.

	IAE	ISE	ITAE	ITSE	max(u)	max(Δu)	J(u)	E [kWh]
PI	12 693	10 448	$1.888{\cdot}10^{8}$	$1.723{\cdot}10^{8}$	100	10	720	0.166
FF classical	5364.9	4927	$6.886{\cdot}10^{7}$	$6.953{\cdot}10^{7}$	100	10	680	0.156
FF STr	5287.7	4927.2	$6.806{\cdot}10^{7}$	$6.974{\cdot}10^{7}$	100	10	700	0.161
FF Gen	**5235.5**	**4916.1**	$\mathbf{6.751{\cdot}10^{7}}$	$6.951{\cdot}10^{7}$	100	10	660	0.152
FF CL	5290.9	4924.8	$6.809{\cdot}10^{7}$	$6.968{\cdot}10^{7}$	100	10	**620**	**0.143**
FF IMC	5269.5	4923.9	$6.790{\cdot}10^{7}$	$6.968{\cdot}10^{7}$	100	10	**620**	**0.143**

Table 8
Performance indices for simulation with data from 21 November 2020.

	IAE	ISE	ITAE	ITSE	max(u)	max(Δu)	J(u)	E [kWh]
PI	10 585	9002.6	$1.484{\cdot}10^{8}$	$1.375{\cdot}10^{8}$	80	10	**320**	**0.074**
FF classical	6129.5	5726.2	$9.065{\cdot}10^{7}$	$8.900{\cdot}10^{7}$	100	20	1360	0.313
FF STr	5984.5	5692.5	$8.874{\cdot}10^{7}$	$8.844{\cdot}10^{7}$	100	20	1340	0.308
FF Gen	6173.6	5745.5	$9.188{\cdot}10^{7}$	$8.917{\cdot}10^{7}$	100	20	1380	0.317
FF CL	**5858.9**	**5672.1**	$\mathbf{8.683{\cdot}10^{7}}$	$\mathbf{8.813{\cdot}10^{7}}$	100	20	1300	0.299
FF IMC	5902.8	5681.2	$8.749{\cdot}10^{7}$	$8.829{\cdot}10^{7}$	100	20	1320	0.304

response of the PI controller. Attending to the performance indices in Table 7, again the FF CL and the FF IMC are the most efficient rules since lower error values can be achieved with reduced control efforts. Surprisingly, in this simulation the lowest IAE value is obtained with the FF Gen, but in exchange for a greater control effort.

Considering that the differences among the feedforward tuning rules can be very slight in some cases, a third simulation was executed to have an additional comparison that could help to determine which should be the techniques to be tested at the real greenhouse. For this third simulation, an ARX model (with similar results to the ones presented in Section 4.3) was identified with data from 21 November 2020. The ARX model was incorporated to the Simulink® model and the results for the control simulations are presented in Fig. 11. In the graphical comparison, it can be noticed the poor performance for the PI controller to reject the disturbances occurring for the external solar radiation between 13:15 and 14:35, while the feedforward strategies produce a more adapting control signals to regulate the inside air temperature in the setpoint. Table 8 contains the performance indices for this simulation, confirming that the best control response is achieved with the FF CL.

After evaluating the simulation results with real data from different days, in the majority of the cases, the FF CL and the FF IMC were the tuning rules with the best overall performance in terms of lower errors and lesser control effort. Hence, these two feedforward tuning rules were selected for the experimental tests at the real greenhouse, considering that the FF STr were already tested in Montoya-Ríos et al. (2020).

To finalize this section, it is important to highlight that, in the previous figures, the feedforward control strategies seem to excellently reject the disturbances due to the simulation results were generated with the ARX models which take into account only the three main climatic disturbances affecting the process output. Therefore, it could be expected that in the real greenhouse, the inside air temperature presented more slight variations around the desired setpoint, as explained in the next section.

4.7. Experimental control tests at the greenhouse

The closed-loop tuning rules for feedforward compensator gains (Veronesi et al., 2017) and the simplified internal model control tuning rules for feedforward controllers (Rodríguez et al., 2020) were tested at the greenhouse under a real state of crop production. On the dates that the tests were performed, the state of the crop was estimated in a leaf area index (LAI) around 3 $m^2_{plants}/m^2_{ground}$. This is a representative value of the predominant size of the plants during a crop season (Rodríguez et al., 2015).

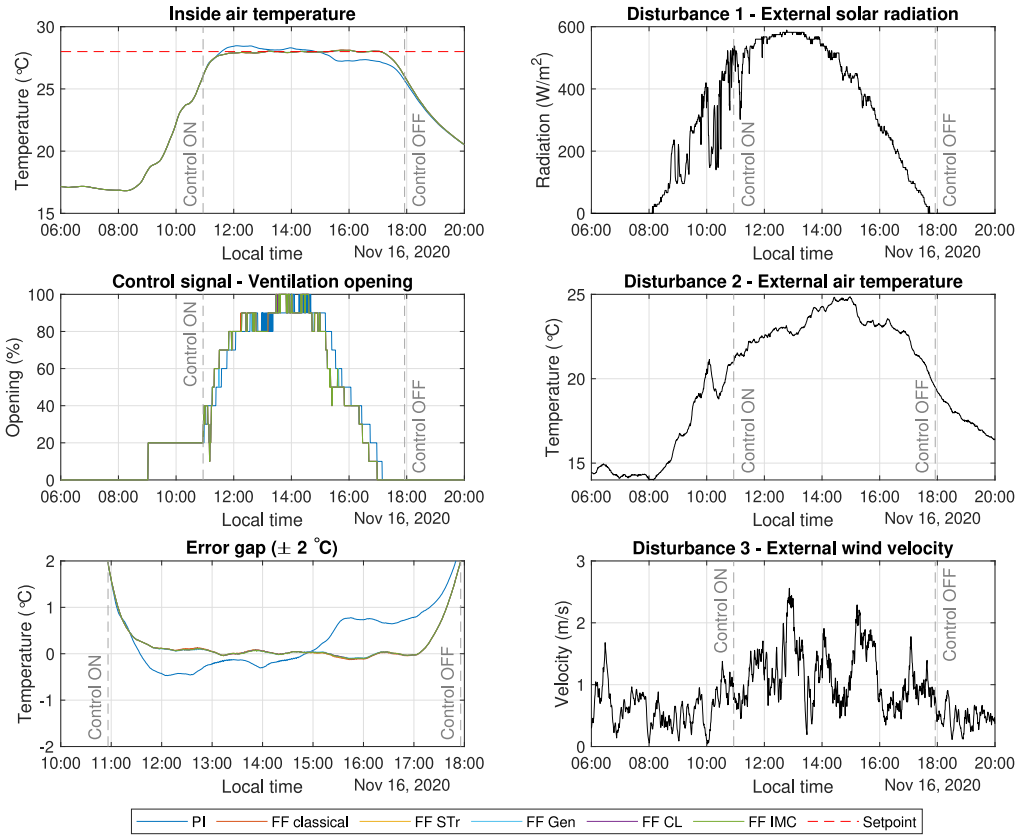

Fig. 10. Results for simulation with data from 16 November 2020.

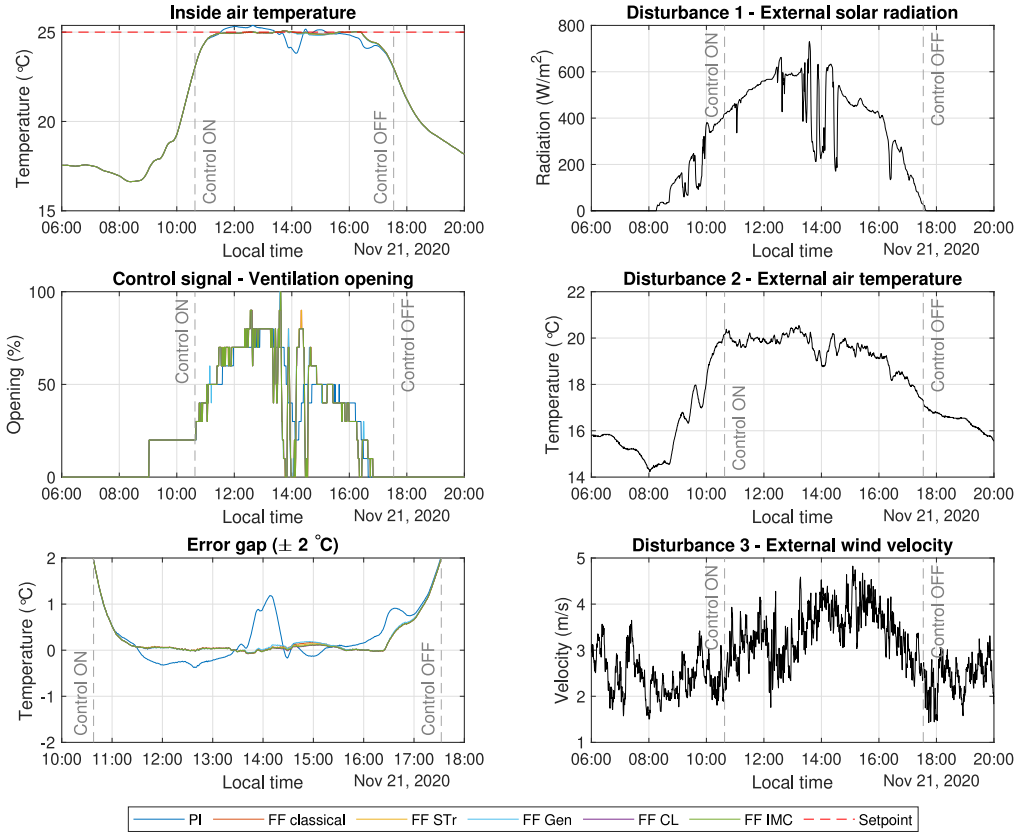

Fig. 11. Results for simulation with data from 21 November 2020.

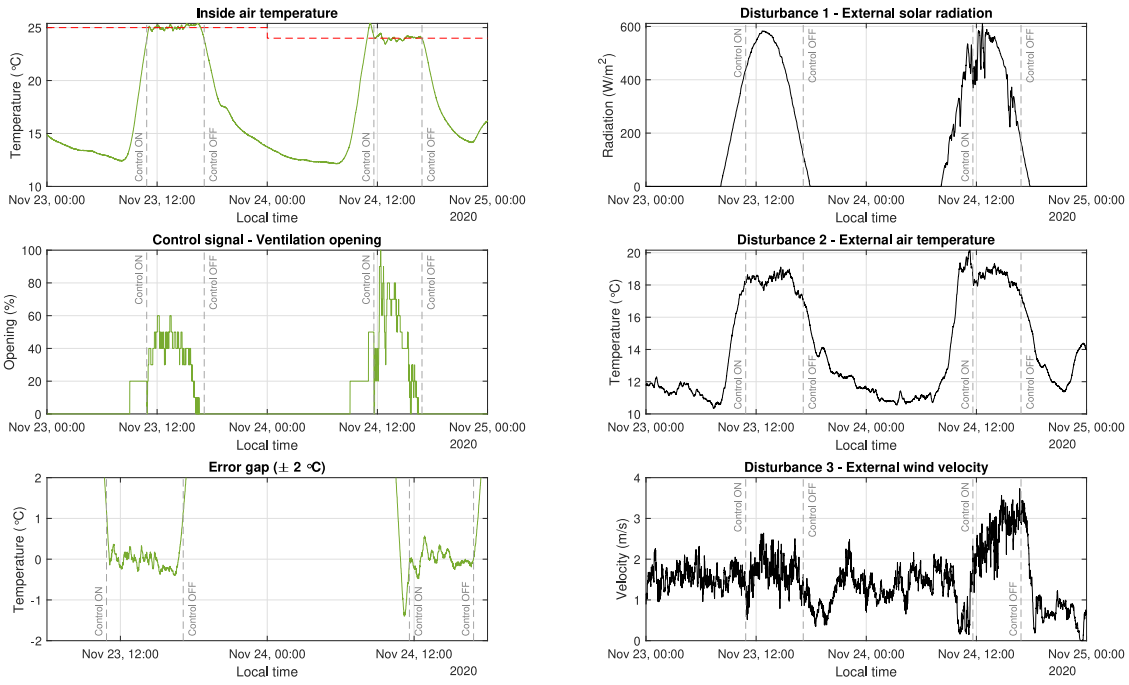

Fig. 12. Results for real experimental tests with the FF IMC tuning rules.

For each tuning rule, two continuous days with experimental results were registered. The PI controller was also tested at the greenhouse to offer a real comparison for the enhanced performance of the feedforward control strategies. Fortunately, for all the experimental tests, a sunny and a cloudy day were recorded, meaning that the performance of each control strategy can be evaluated with and without the presence of heavy disturbances.

The control tests were executed by programming a MATLAB® script in the supervisory control and data acquisition (SCADA) system of the greenhouse. To that end, the feedforward compensators (FF CL and FF IMC from Table 3) were recalculated in discrete-time form. The sample time for the control loop was imposed as 30 s. The anti-windup and the bumpless transfer mechanisms were also coded in the MATLAB® script, allowing an easy activation of the desired control strategy for the daytime. The values for the setpoints were manually fixed between 23 °C and 25 °C, according to the typical temperature ranges for the crop during autumn in the southeast of Spain (Rodríguez et al., 2015).

The results for the FF IMC are presented in Fig. 12. For the first day, 23 November 2020, the weather conditions were calm and the small disturbances from the external air temperature and the external wind velocity were adequately compensated by the feedforward control. The inside air temperature was controlled at 25 °C, and the control error during the test was contained in a interval smaller than ±0.4 °C. For the second day, 24 November 2020, the weather conditions presented more noticeable changes and the control signal reveals that the feedforward action was essential to reject the changes in the external solar radiation during the first hours after the daytime control was activated. Some oscillations for the inside air temperature can be observed, but the overall performance is remarkable considering that the error was limited to an interval smaller than ±0.6 °C around the setpoint at 23 °C.

The results for the FF CL are presented in Fig. 13. The first day that these tuning rules were tested, 28 November 2020, the weather conditions were very similar to the previously shown for 23 November 2020, being both sunny days. Hence, an almost identical behaviour was obtained, regulating the inside air temperature at 25 °C. In this test, the control error was contained in an interval of ±0.6 °C, probably due to the larger amplitude of the changes in the external wind velocity. The second day, 29 November 2020, was a cloudy day, with abrupt disturbances from the external solar radiation during the first instants after the control strategy was activated, as occurred on 24 November 2020. However, on 29 November 2020, the amplitude of the changes for the solar radiation was considerable. For instance, the solar radiation decreased from 514 W/m^2 to 200 W/m^2 in 10 min, causing the control signal to close the windows to avoid a drop in the inside air temperature. Also, a sudden increase in the solar radiation occurred at 11:30, changing from 200 W/m^2 to 600 W/m^2 in 30 min. The control signal tried to open the ventilation progressively until a 100% of opening was reached and it saturated for 15 min. This explains why the inside air temperature deviated from the setpoint at 12:00. Thanks to the combined action of the feedforward compensators and the anti-windup mechanism, the error for this test was contained in an interval of ±1 °C.

Fig. 14 presents the results for the PI controller without the addition of any feedforward compensator. For the first day of test, 1 December 2020, the strong disturbances occurring for the external weather variables affected the control performance. Without the feedforward action, the disturbance effects were not well rejected by the feedback controller, which offered a slower response. The inside air temperature deviated from the setpoint (24 °C) and the control error was contained in an interval of ±2 °C. For the second day of test, 2 December 2020, the external meteorological conditions were more calm, and the inside air temperature did not present relevant oscillations around the setpoint. In this case the error was limited to an interval of ±0.7 °C. The control signal for the ventilation was mainly evolving to compensate the variations for the external air temperature and the wind velocity.

The performance indices for all the real tests are shown in Table 9. Although the weather conditions and the duration of the control tests were different for each day, some conclusions can be drawn. To facilitate the quantitative comparison, the error indices were calculated using the sampled data every 30 s and the results were divided by the duration of each test. The best overall performance in terms of lower error values is obtained with the FF IMC. A similar behaviour was observed for the FF CL, in this case with lesser control effort indices but with greater error values. As expected, the PI controller presented the worst error indices, especially for the ITAE and ITSE, confirming its difficulties to regulate the inside air temperature close to the setpoint for the duration of the control tests.

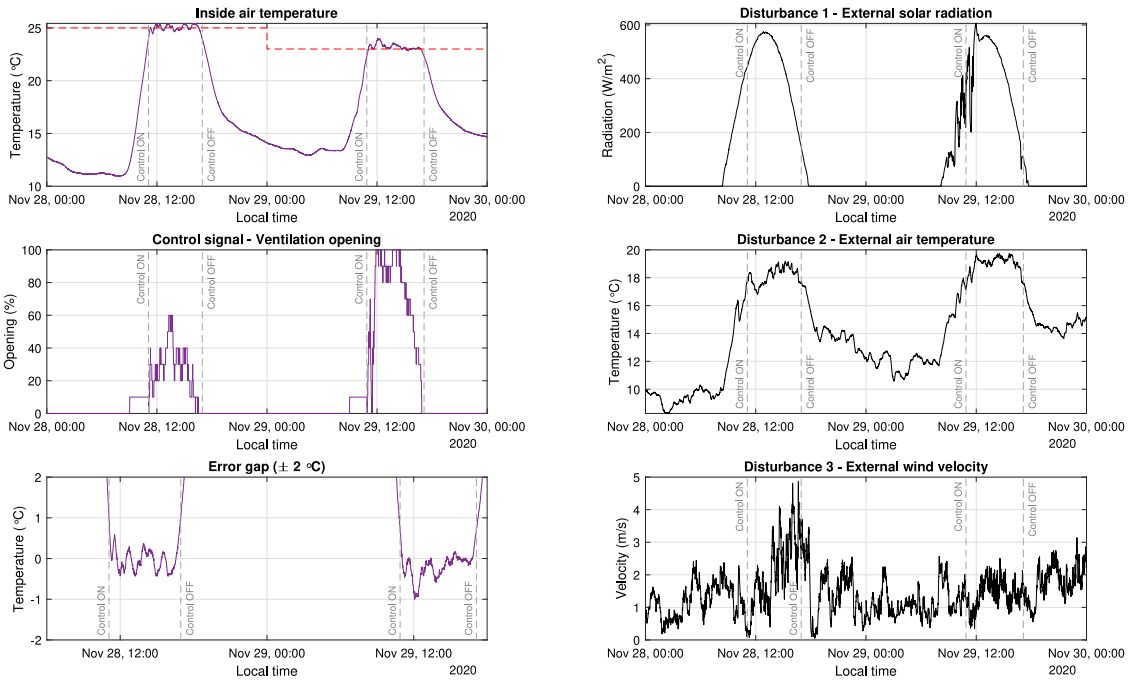

Fig. 13. Results for real tests with the FF CL tuning rules.

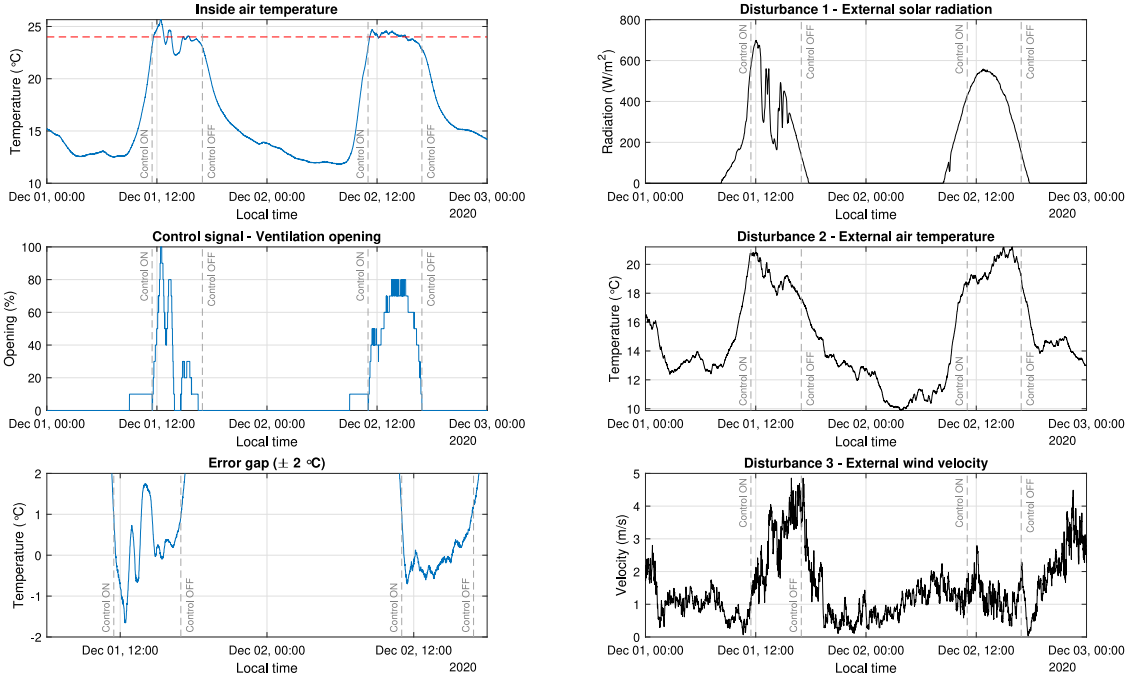

Fig. 14. Results for real tests with the PI controller.

As expected from Section 4.6, in the real tests, the inside air temperature presented slight variations around the setpoint due to the effect of other non-measurable disturbances and modelling uncertainties. Nevertheless, the feedforward control strategies offered a noteworthy performance considering that the perfect cancellation for the disturbances was not possible because of the simplifications to obtain the feedforward compensators preventing the non-realizable delay inversion.

Attending to the estimated energy index, the electrical consumption of the PI controller in the real greenhouse is similar to the electrical consumption of the feedforward control strategies. However, the inclusion of the feedforward compensators guarantees a more desirable control response for the inside air temperature, with less variations that could affect the crop, as the disturbances are better rejected. So, considering the lower error values for the feedforward control strategies and a comparable energy consumption to the PI controller,

Table 9
Performance indices for the real tests at the greenhouse.

FF IMC									
	Duration	IAE/h	ISE/h	ITAE/h	ITSE/h	max(u)	max(Δu)	J(u)	E [kWh]
Nov 23, 2020	6.3 h	669.26	238.75	$8.708{\cdot}10^6$	$3.338{\cdot}10^6$	60	10	780	0.179
Nov 24, 2020	5.2 h	658.09	211.17	$6.539{\cdot}10^6$	$2.325{\cdot}10^6$	100	50	870	0.200
FF CL									
	Duration	IAE/h	ISE/h	ITAE/h	ITSE/h	max(u)	max(Δu)	J(u)	E [kWh]
Nov 28, 2020	5.9 h	853.77	305.05	$9.354{\cdot}10^6$	$3.531{\cdot}10^6$	60	10	630	0.145
Nov 29, 2020	6.2 h	917.49	454.74	$7.737{\cdot}10^6$	$3.234{\cdot}10^6$	100	10	820	0.189
PI									
	Duration	IAE/h	ISE/h	ITAE/h	ITSE/h	max(u)	max(Δu)	J(u)	E [kWh]
Dec 01, 2020	5.5 h	2337.27	2504.36	$2.009{\cdot}10^7$	$2.025{\cdot}10^7$	100	10	510	0.117
Dec 02, 2020	5.9 h	1231.53	609.15	$1.387{\cdot}10^7$	$7.651{\cdot}10^6$	80	10	850	0.195

it can be deduced that the feedforward control strategies are more efficient for a full crop season.

5. Conclusions

In this paper, the relevant characteristics for different feedforward tuning rules have been summarized. A distinctive aspect of this work is the application of the tuning rules to control the inside air temperature in a greenhouse. In this context, a practical comparison for feedforward tuning rules has been presented for the case when the delay inversion is non-realizable. The feedforward compensators were applied to the rejection of disturbances that affect the process output. A series of simulations and real tests were performed to provide graphical and quantitative comparisons. All the tuning rules were compared against a PI controller and the classical open-loop design method for feedforward compensators.

The simulation tests confirm that selecting the most adequate feedforward tuning rule and the control scheme principally depends on the system dynamics and the type of disturbance to reject. In this sense, it is difficult to propose a guideline to select the "best" tuning rule, moreover considering that in real processes combinations of step-like and ramp-like disturbances can appear. Nonetheless, for the classical control scheme, it may be advisable to use the FF CL or the FF IMC tuning rules, due to their simplicity in tuning only the compensator gain and their consistency in presenting lower error values with lesser control effort. Additionally, an interesting result was observed for the classical feedforward tuning rule, achieving a complete rejection for ramp disturbances, even if the ideal compensator is non-realizable. Hence, it has been demonstrated that the classical feedforward method can be a valid strategy to reject ramp disturbances instead of introducing an extra integrator in the feedback controller.

Furthermore, taking into account that in most cases the calculated compensators have the same structure (e.g. lead–lag filters), it is interesting to observe how the different tuning rules try to offer optimal values for the compensator parameters to satisfy a trade-off between error minimization and control effort. For instance, the majority of the tuning rules impose $\tau_z = \tau_u$ for the sake of simplicity. However, as mentioned for the FF HH tuning rules, adjusting the zero of the compensator could offer a better performance in some cases. Therefore, the poles and zeros of the "optimal" feedforward compensator can vary in a region conditioned by the minimization of a desired error index.

In conclusion, the experimental tests performed at the real greenhouse presented outstanding results for disturbances rejection when compared to the feedback controller responses without the inclusion of the feedforward compensators. The feedforward control strategies based on the novel tuning rules offered an efficient behaviour in terms of control effort and energy consumption. These feedforward controllers were successful in regulating the inside air temperature of the greenhouse closer to the desired setpoint, even with the presence of strong disturbances, and even with noisy signals as noticed for the external wind velocity. The experimental results demonstrate the suitability of using these types of feedforward tuning rules to effectively deal with the problems of non-realizable delay inversion in real processes.

Declaration of competing interest

The authors declare that they have no known competing financial interests or personal relationships that could have appeared to influence the work reported in this paper.

Acknowledgements

This work was supported by the National R+D+i Plan Project DPI2017-85007-R of the Spanish Ministry of Science, Innovation and Universities and ERDF funds. Author F. García-Mañas is supported by an FPU grant of the Spanish Ministry of Science, Innovation and Universities. Authors also want to express their gratitude to the staff of "Las Palmerillas" Experimental Station of the Cajamar Foundation.

References

Åström, K. J., & Hägglund, T. (2006). *Advanced PID control*. ISA-The Instrumentation, Systems, and Automation Society.

Berenguel, M., Yebra, L. J., & Rodríguez, F. (2003). Adaptive control strategies for greenhouse temperature control. In *2003 European control conference (ECC)* (pp. 2747–2752). http://dx.doi.org/10.23919/ECC.2003.7086457.

Boerlage, M., Steinbuch, M., Lambrechts, P., & van de Wal, M. (2003). Model-based feedforward for motion systems. In *Proceedings of 2003 IEEE conference on control applications, 2003. CCA 2003. Vol. 2* (pp. 1158–1163). http://dx.doi.org/10.1109/CCA.2003.1223174.

Brosilow, C., & Joseph, B. (2002). *Techniques of model-based control*. Prentice Hall Professional.

Corless, R. M., Gonnet, G. H., Hare, D. E. G., Jeffrey, D. J., & Knuth, D. E. (1996). On the LambertW function. *Advances in Computational Mathematics*, *5*(1), 329–359. http://dx.doi.org/10.1007/BF02124750.

Fourati, F., & Chtourou, M. (2007). A greenhouse control with feed-forward and recurrent neural networks. *Simulation Modelling Practice and Theory*, *15*(8), 1016–1028. http://dx.doi.org/10.1016/j.simpat.2007.06.001.

Gruber, J. K., Guzmán, J. L., Rodríguez, F., Bordons, C., Berenguel, M., & Sánchez, J. A. (2011). Nonlinear MPC based on a Volterra series model for greenhouse temperature control using natural ventilation. *Control Engineering Practice*, *19*(4), 354–366. http://dx.doi.org/10.1016/j.conengprac.2010.12.004.

Gurban, E. H., & Andreescu, G.-D. (2012). Comparison study of PID controller tuning for greenhouse climate with feedback-feedforward linearization and decoupling. In *2012 16th international conference on system theory, control and computing (ICSTCC)* (pp. 1–6).

Guzmán, J. L., & Hägglund, T. (2011). Simple tuning rules for feedforward compensators. *Journal of Process Control*, *21*(1), 92–102. http://dx.doi.org/10.1016/j.jprocont.2010.10.007.

Guzmán, J. L., Hägglund, T., Veronesi, M., & Visioli, A. (2015). Performance indices for feedforward control. *Journal of Process Control*, *26*, 26–34. http://dx.doi.org/10.1016/j.jprocont.2014.12.004.

Guzmán, J. L., Hägglund, T., & Visioli, A. (2012). Feedforward compensation for PID control loops. In *PID control in the third millennium* (pp. 207–234). Springer, http://dx.doi.org/10.1007/978-1-4471-2425-2_7.

Hast, M., & Hägglund, T. (2014). Low-order feedforward controllers: Optimal performance and practical considerations. *Journal of Process Control*, *24*(9), 1462–1471. http://dx.doi.org/10.1016/j.jprocont.2014.06.016.

Iddio, E., Wang, L., Thomas, Y., McMorrow, G., & Denzer, A. (2020). Energy efficient operation and modeling for greenhouses: A literature review. *Renewable and Sustainable Energy Reviews*, *117*, Article 109480. http://dx.doi.org/10.1016/j.rser.2019.109480.

Lambrechts, P., Boerlage, M., & Steinbuch, M. (2005). Trajectory planning and feedforward design for electromechanical motion systems. *Control Engineering Practice*, *13*(2), 145–157. http://dx.doi.org/10.1016/j.conengprac.2004.02.010.

Montoya-Ríos, A. P., García-Mañas, F., Guzmán, J. L., & Rodríguez, F. (2020). Simple tuning rules for feedforward compensators applied to greenhouse daytime temperature control using natural ventilation. *Agronomy*, *10*(9), 1327. http://dx.doi.org/10.3390/agronomy10091327.

Pawlowski, A., Guzmán, J. L., Normey-Rico, J. E., & Berenguel, M. (2012). Improving feedforward disturbance compensation capabilities in generalized predictive control. *Journal of Process Control*, *22*(3), 527–539. http://dx.doi.org/10.1016/j.jprocont.2012.01.010.

Piccagli, S., & Visioli, A. (2009). An optimal feedforward control design for the set-point following of MIMO processes. *Journal of Process Control*, *19*(6), 978–984. http://dx.doi.org/10.1016/j.jprocont.2008.12.010.

Rodríguez, C., Aranda-Escolástico, E., Guzmán, J. L., Berenguel, M., & Hägglund, T. (2020). Revisiting the simplified internal model control tuning rules for low-order controllers: feedforward controller. *IET Control Theory & Applications*, *14*(12), 1612–1618. http://dx.doi.org/10.1049/iet-cta.2019.0823.

Rodríguez, F., Berenguel, M., & Arahal, M. R. (2001). Feedforward controllers for greenhouse climate control based on physical models. In *2001 European control conference (ECC)* (pp. 2158–2163). http://dx.doi.org/10.23919/ECC.2001.7076243.

Rodríguez, F., Berenguel, M., Guzmán, J. L., & Ramírez-Arias, A. (2015). *Modeling and control of greenhouse crop growth*. Springer, http://dx.doi.org/10.1007/978-3-319-11134-6.

Rodríguez, C., Guzmán, J. L., Berenguel, M., & Hägglund, T. (2013). Generalized feedforward tuning rules for non-realizable delay inversion. *Journal of Process Control*, *23*(9), 1241–1250. http://dx.doi.org/10.1016/j.jprocont.2013.08.001.

Rodríguez, C., Guzmán, J. L., Berenguel, M., & Hägglund, T. (2014). Optimal feedforward compensators for systems with right-half plane zeros. *Journal of Process Control*, *24*(4), 368–374. http://dx.doi.org/10.1016/j.jprocont.2014.02.014.

Rodríguez, C., Normey-Rico, J. E., Guzmán, J. L., & Berenguel, M. (2016). Robust design methodology for simultaneous feedforward and feedback tuning. *IET Control Theory & Applications*, *10*(1), 84–94. http://dx.doi.org/10.1049/iet-cta.2015.0154.

Rojas, J. D., & Vilanova, R. (2009). Feedforward based two degrees of freedom formulation of the Virtual Reference Feedback Tuning approach. In *2009 European control conference (ECC)* (pp. 1800–1805). http://dx.doi.org/10.23919/ECC.2009.7074664.

del Sagrado, J., Sánchez, J. A., Rodríguez, F., & Berenguel, M. (2016). Bayesian networks for greenhouse temperature control. *Journal of Applied Logic*, *17*, 25–35. http://dx.doi.org/10.1016/j.jal.2015.09.006.

Speetjens, S. L., Stigter, J. D., & Van Straten, G. (2009). Towards an adaptive model for greenhouse control. *Computers and Electronics in Agriculture*, *67*(1–2), 1–8. http://dx.doi.org/10.1016/j.compag.2009.01.012.

Su, Y., Yu, Q., & Zeng, L. (2020). Parameter self-tuning PID control for greenhouse climate control problem. *IEEE Access*, *8*, 186157–186171. http://dx.doi.org/10.1109/ACCESS.2020.3030416.

Veronesi, M., Guzmán, J. L., Visioli, A., & Hägglund, T. (2017). Closed-loop tuning rules for feedforward compensator gains. *IFAC-PapersOnLine*, *50*(1), 7523–7528. http://dx.doi.org/10.1016/j.ifacol.2017.08.1186.

Veronesi, M., & Visioli, A. (2014). Automatic tuning of feedforward controllers for disturbance rejection. *Industrial and Engineering Chemistry Research*, *53*(7), 2764–2770. http://dx.doi.org/10.1021/ie403089f.

Vilanova, R., Arrieta, O., & Ponsa, P. (2009). IMC based feedforward controller framework for disturbance attenuation on uncertain systems. *ISA Transactions*, *48*(4), 439–448. http://dx.doi.org/10.1016/j.isatra.2009.05.007.

Visioli, A. (2004). A new design for a PID plus feedforward controller. *Journal of Process Control*, *14*(4), 457–463. http://dx.doi.org/10.1016/j.jprocont.2003.09.003.